RSC Advances

ROYAL SOCIETY OF CHEMISTRY

www.rsc.org/advances

Piezoelectric sodium potassium niobate mediated improved polarization and *in vitro* bioactivity of Hydroxyapatite

Ashutosh Kumar Dubey,* Ryota Kinoshita and Ken-ichi Kakimoto

Department of Materials Science and Engineering, Graduate School of Engineering, Nagoya Institute of Technology, Gokiso-cho, Showa-ku, Nagoya 466-8555, Japan.

Abstract

The present work reports the effect of lamination of biocompatible lithium sodium potassium niobate [$Li_{0.06}(Na_{0.5}K_{0.5})_{0.94}NbO_3$, LNKN] multilayered tapes between hydroxyapatite (HA) layers on the dielectric and electrical properties of HA. The LNKN tapes were laminated between HA layers via various buffer interlayers. It has been found that for the optimal molar ratio, X = 3~7 of LNKN in the LNKN:HA (X:1) buffer interlayer, good adhesion between HA and LNKN layers were observed. The effect of lamination of buffer and HA layers and subsequent sintering on the dielectric and electrical properties of inserted ferroelectric LNKN has been evaluated after removing these laminated layers from the composite (HB-LNKN). The crystal structure of HB-LNKN has been changed from tetragonal to orthorhombic phase. In addition, the dielectric measurement suggests that the tetragonal region, i.e., the range between T_{O-T} and T_C for HB-LNKN has also been reduced as compared to that of as-sintered LNKN. The variation in tetragonal region in HB-LNKN has been found to depend on the composition (X) of the buffer layer in the parent laminated composite. For the buffer layer composition, X = 7, the improved piezoelectric (d_{33} = 104 pC/N) as well as ferroelectric (E_c = 11 kV/cm, P_{max} = 23 $\mu C/cm^2$) response of HB-LNKN was observed. The associated polarization mechanisms in context of ferroelectric LNKN have also been explored. About 6 times increase in the polarizability of HA (for X = 7) is obtained without affecting its biocompatibility by the proposed concept of the laminated composite. In addition, the developed laminated composite is piezoelectric (d_{33} = 2 pC/N) in nature, like living bone. Further, the effect of increased

polarizability of hydroxypatite (for X = 7) on the *in vitro* bioactivity has been examined after immersing in simulated body fluid (SBF) for 3, 7 and 14 days, respectively. The augmented polarizability of HA almost doubled the apatite formation rate in SBF.

Keywords: Hydroxyapatite, Sodium potassium niobate, Electrical properties, Bioactivity.

*Correspondence: akdbhu@gmail.com (A.K. Dubey) Tel. & Fax: +81 52 735 7734

1. Introduction

Hydroxyapatite (HA) is well established outstanding biocompatible material owing to the chemical correspondence with the bone mineral, which facilitates direct bonding with the bone without any foreign body reaction.[1-6] However, HA does not meet the mechanical and electrical assets of the natural bone. The presence of piezoelectric,[7,8] pyroelectric[9] as well as ferroelectric[10] properties in the living bone control it's metabolism.[11-14] Hastings et al.[15] suggested the analogy of bone as the structure consisting of domains, the dipoles of which can be preferentially aligned by means of the electrical or mechanical stimulus. By virtue of piezoelectricity, the bone polarizes in response to applied mechanical stress which plays a key role in the controlled bone growth.[16] The polarity depends upon the stress direction, compressively stressed bone region polarizes negatively and vice-versa.[17] Mcelhaney et al.[18] demonstrated that the amount and nature of charge generated in the human femur due to the mechanical stress are different at various locations and directions. The negatively polarized surfaces have been shown to enhance the bone formation by stimulating the bone-cell activity.[19,20] The development of negative potential also helps in the faster healing of the fractured bones.[21] The application external electrical potential gradient has been demonstrated to increase the bone mineral density.[22] The negatively polarized surfaces of HA accelerates the growth of bone-like crystals in simulated body fluid.[23,24]

It has been established that the current generated due to the mechanical loading of ferroelectrics biocompatible ceramics increases the interfacial bonding between the implant and bone tissue.[25,26] Apart from the improved bioactivity, the incorporation of piezoelectric phase in ceramic matrix enhances the fracture toughness of the composite system.[27,28] Therefore, it is of potential interest to develop the ferroelectric biomedical implant in order to realize the improved biological performance.

The sodium potassium niobate ($Na_{0.5}K_{0.5}NbO_3$, NKN) illustrates reasonably attractive electrical properties such as piezoelectric strain coefficient (~160 pC/N), electromechanical coupling coefficient (0.44) etc. among the lead-free piezoelectric ceramics.[29] The NKN ($Na_xK_yNbO_3$; $0 \leq x \leq 0.8$ and $0.2 \leq y \leq 1$) has been suggested as a potential biocompatible material.[30] The Nb coated surfaces demonstrate a better response for bone cells as compared to it's uncoated counter-substrate.[31] The Li-substitution at A-site [Li_x $(Na_{0.5}K_{0.5})_{1-x}NbO_3$; x ~ 0.06, LNKN] has been reported to enhance the polarizability of NKN.[32]

In view of the various consequences of the electromechanical response of the natural bone, the present work attempted to improve the electrical activities of HA without affecting its biocompatibility by inserting the tape casted LNKN sheets between the HA layers through buffer interlayers and subsequent consolidation. The effect of lamination and sintering of buffer and HA layers on the dielectric and electrical properties of inserted LNKN layer has also been studied. Further, the effect of improved electrical activities of HA on *in vitro* bioactivity has been demonstrated.

2. Experimental

2.1 Materials Processing

The synthesis procedure for $Li_{0.06}(Na_{0.5}K_{0.5})_{0.94}NbO_3$ (LNKN) has been described elsewhere.[33] Briefly, LNKN was consolidated via solid state ceramic route using the high purity (99.99%) starting powders, Li_2CO_3, Na_2CO_3, Nb_2O_5 and K_2CO_3. The HA powder was obtained from Kishida Chemicals (Osaka, Japan). The laminated samples were fabricated by tape casting (doctor blade) technique (IMC-70F0-B, Imoto Machinery Co., Ltd., Japan). The slurry of each constituent was prepared in a polypropylene container and stirred using automated planetary centrifugal mixer (ARE-310, Thinky Corporation, Tokyo, Japan) at a rotation speed of 2200 rpm

for 1 min, followed by 2000 rpm for 30 sec. The LNKN slurry was obtained using the calcined LNKN powder, Olycox binder (Kyoeisha Chemical Co. Ltd, Osaka, Japan) and acetone in weight ratio of 5.0:4.0:0.4. However, the weight ratios of HA powder, Olycox binder and acetone in HA slurry was 2:5:1. The slurry for the buffer tape was the mixture of LNKN and HA powders [in the molar ratio of X: 1 (X= 1~9)], binder and acetone in the weight ratio of 2:3:1. This combination provides flexibility to the tapes, suitable for molding without any crack formation. The respective slurry was poured on the carrier film and the green tapes were casted at a casting speed of 2 cm/sec with the blade height of 200 μm. The tapes were cut into squares of side 1.5 mm and stacked in order of HA-LNKN-HA/HA-buffer-LNKN-buffer-HA. The laminated composite contains 10, 10 and 40 tape casted sheets for HA, buffer and LNKN layers, respectively. The laminated tapes were dried overnight, uniaxially pressed at 22 MPa and then fired at 800^0C to burn out the binder. Finally, the samples were cold isostatically pressed at 200 MPa, which was followed by sintering at 1082^0C for 2 h.

2.2 Phase evaluation and microstructural analyses

The phases present in the laminated compacts were detected using X-ray diffraction (XRD) patterns (Rigaku RAD-C). The microstructural and compositional analyses were performed for the polished and platinum/gold deposited samples using scanning electron microscope (SEM, Tiny SEM, Mighty-8) and energy dispersive X-ray spectroscopy (EDX, Tiny-EDXS), respectively.

2.3 Dielectric and electrical characterization

The dielectric properties of the samples were evaluated using LCR meter (NF ZM2355). The capacitance and dielectric loss was measured in the temperature and frequency ranges of 25-550^0C and 0.1 Hz - 100 kHz, respectively. The samples were polarized using corona discharge

gun at 16 kV for 1 min with the needle shaped electrode, placed at 1 mm distance from the sample surface. The piezoelectric strain coefficient (d_{33}) was measured using d_{33} meter (Academia Sinica, ZJ-6B). For the measurement of PE hysteresis loop, the ferroelectric tester was used (aixACCT TF2000FE-HV).

2.4 *In vitro* bioactivity evaluation

The *in vitro* bioactivity of unpolarized and corona polarized samples (4x4 mm^2) was examined using XRD analysis and SEM observations, after soaking in simulated body fluid (SBF)[34,35] for 3, 7 and 14 days, respectively at temperature of 37^oC.

3. Results and Discussion

3.1 Lamination and sintering of the tape casted sheets

Initially, the composite was prepared by laminating LNKN and HA tapes as HA-LNKN-HA and subsequent firing. After sintering, the HA and LNKN layers were peeled off due to the different thermal shrinkage behavior of HA and LNKN. The coefficients of the thermal expansion of HA and NKN are reported to be $14x10^{-6}/^0C$[36] and $8x10^{-6}/^0C$,[37] respectively.

In order to improve adhesion, difference in the thermal shrinkage was compensated by inserting a buffer layer between HA and LNKN layers. The buffer layer contains the mixture of LNKN and HA in the molar ratio of X: 1 (X = 1 ~ 9). For the optimal values of X (3~7), good adhesion was observed without any crack at the interfacial regions. The XRD results confirmed the formation of single phase (HA) for both the sintered monolithic HA as well as laminated composites (not shown).

Fig. 1(a) represents the SEM image of the cross section of laminated (HA-buffer-LNKN-buffer-HA) composite sample for the buffer layer composition, X = 7. At the interfacial region between the buffer and LNKN layers, dissimilar microstructure from either of the phases is observed. The

EDS analysis suggests that Ca is diffused into LNKN layer during the processing, which was detected upto few tens of micrometers from the interfacial region between the buffer and LNKN. The thickness of reaction layer is found to depend on the composition of the buffer layer. With increase in molar ratio (X) of LNKN in the buffer layer, thickness of the reaction layer decreases [Fig. 1 (b)]. For X = 1, thickness of the reaction layer is measured to be 37 μm, which decreases up to 23 μm for X = 7. It can, therefore, be suggested that higher molar ratio of LNKN phase in the buffer layer can suppress the reaction between HA and LNKN phases.

3.2 Electrical properties of laminated LNKN layer

In order to reveal the effect of lamination of HA and buffer layers and subsequent sintering on the electrical properties of the LNKN, the electrical properties of as-sintered LNKN (abbreviated as AS-LNKN) as well as the LNKN, obtained after removing the HA and buffer layers from the sintered laminated composite (abbreviated as HB-LNKN), were studied. About 1 mm thick LNKN pellets were obtained after removing both the HA and buffer layers from the laminated composite.

Fig. 2 (a) illustrates that the XRD patterns of AS-LNKN and HB-LNKN are different. A comparison with the base material $KNbO_3$ suggests that the crystal system of HB-LNKN has been changed from tetragonal (for AS-LNKN) to orthorhombic. In addition, a secondary phase, $K_{2.6}Nb_{11.6}O_{30}$ is detected in HB-LNKN, which is a compound formed for deficient A site (Na, K) in NKN [Fig. 2 (b)].

Fig. 3 (a) demonstrates the temperature dependent dielectric behavior of AS-LNKN as well as HB-LNKN for the buffer layer composition, X = 7 in the parent composite. From the figure, it is clear that the transition temperatures for orthorhombic to tetragonal (T_{O-T}) as well as tetragonal to cubic (T_C) phases are different in both the cases. In case of HB-LNKN, the T_{O-T} shifted

towards the higher temperature side by 61^0C (from 15 to 76^0C) and T_C shifted towards lower temperature side by 20^0C (from 456 to 436^0C) from those of the AS-LNKN. Therefore, the tetragonal region, i.e., the range between T_{O-T} and T_C for HB-LNKN has been reduced. The tetragonal region increases with increase in Li content in the solid solution LNKN.[32] Therefore, reduction of the tetragonal region in the present case is associated with the decrease in solid solubility of Li in NKN phase. In addition, the tetragonal region is also found to depend on the composition (X) of the buffer layer [Fig. 3(b)] in the parent laminated composite. It can, therefore, be suggested that the Li content in the solid solution HB-LNKN has changed by changing the buffer layer composition (X) in the laminated composite. For the buffer layer with compositions, X = 1, 3 and 5, temperature range between T_{O-T} and T_C are 330, 319 and 324^0C, respectively. It has been estimated that the Li content in these solid solutions is about 3 mol.%. On the other hand, for the compositions, X = 7 and 9, temperature range between T_{O-T} and T_C are 359 and 345^0C, respectively, which corresponds to about 4 mol. % Li in the solid solution LNKN. Therefore, the buffer layer with composition, X > 5 is expected to provide better response as far as the polarizability of the HB-NLKN is concerned. From the above results, it can be concluded that with increase in composition (X) of the buffer layer, solid solubility of Li in HB-LNKN increases. The decrease in the Li content from the HB-LNKN solid solution is probably due to diffusion of Li into the adjacent layers, which can be reduced by increasing the composition (X) of buffer layer in the parent laminated composite. For higher values of X (6 ~ 9), the minimal diffusion of Li and Ca is observed.

As evident from the Fig. 4, the resistivity of the HB-LNKN sample varies with the composition (X) of the buffer layer in parent laminated composite. The samples with the compositions, X = 1~5 show lower resistivity (10^8-10^9 ohm-cm) as compared to the samples with compositions, X

= 6~9 (10^9-10^{11} ohm-cm) because of the diffusion of Li and Ca into the adjacent layers. These diffusions can induce A-site defect in HB-LNKN and hence, lower the electrical resistivity.

Fig. 5 illustrates the PE hysteresis behavior for AS-LNKN [Fig. 5 (a)] as well as HB-LNKN [Figs. 5 (b)-(h)] with the varying composition (X = 1~ 9) of the buffer layer in the corresponding parent composites. In case of the HB-LNKN samples with low resistivity (for X = 1~5), the leakage current is large. However, the higher resistivity samples (for X = 6~9) demonstrate the saturated hysteresis loop. The coercive field (E_c) and maximum polarization (P_{max}) values for AS-LNKN sample are 16.0 kV/cm and 24.1 μC/cm^2, respectively. However, the values of E_c and P_{max} for HB-LNKN samples with the compositions, X = 6, 7, 8 and 9 are (11.0, 11.3, 12.5, 11.0) kV/cm and (16.0, 23.0, 18.0, 16.7) μC/cm^2, respectively. The P_{max} value for HB-LNKN sample with composition, X = 7 closely resembles with that of the AS-LNKN sample.

In addition, a large dispersion in dielectric constant and loss with frequency is obtained for the compositions, X = 1~5 at lower frequencies (< 100 Hz) as depicted by the lower resistivity of the sample [Fig. 6(a)]. The sharp decrease in dielectric constant and loss is associated with the space charge polarization. Fig. 6 (b) shows the variation of dielectric constant and loss for HB-LNKN sample with the molar ratio (X) of LNKN in buffer layer. A very high value of dielectric constant and loss are observed for the compositions, X = 1~5 as compared to those for X = 7~9. From Figs. 6 (a) and (b), it is clear that the samples with compositions, X = 1~5 have significant conductivity. However, the samples with compositions, X = 7~9 reveal the intrinsic contribution of dielectric response.

The piezoelectric properties of the samples were measured after poling with the field strength of 3 kV/mm for 30 min in Si oil at a temperature of 75^{0}C. Fig. 7 represents the variation of piezoelectric strain coefficient (d_{33}) of HB-LNKN samples with the various buffer layer

composition (X) in the parent composite. With increase in the composition (X) from X = 1 to X = 7, the d_{33} increases up to 104 pC/N from 59 (X = 1) and reduced thereafter to 66 pC/N (X = 9). The increase in d_{33} value is associated with the increase of the solid solubility of Li in NKN phase.

These results suggest that the diffusion of Li and Ca elements at the buffer layer/LNKN interface affects the electrical properties of HB-LNKN. To demonstrate the effect of diffusion of Li and Ca elements on the electrical properties of HB-LNKN, the thickness of HB-LNKN sample was reduced from 1 mm to 0.5 mm and their electrical properties were compared.

Fig. 8 plots the XRD patterns of both the HB-LNKN samples. The intensities of the diffraction peaks, corresponding to the secondary phase $K_{2.6}Nb_{11.6}O_{30}$, reduced significantly for the 0.5 mm thick HB-LNKN sample. From this result, the diffusion of Li and Ca elements in the vicinity of LNKN layer can be verified. Table 1 compares the dielectric constant, loss, electrical resistivity and piezoelectric coefficient (d_{33}) values for the HB-LNKN samples with the thicknesses of 1 and 0.5 mm, respectively, for the compositions, X = 6 and 7. From table, it is clear that the dielectric and electrical properties are improved significantly after reducing the thickness of the HB-LNKN disc (for X = 7). Also, the increased resistivity indicates minimal diffusion of the Li and Ca into the adjacent layers.

The variation in Li content in LNKN ceramics has substantial effect on the structure, dielectric and electrical properties of alkali niobate ceramics. Guo et al.[32] demonstrated that piezoelectric ceramic $[Li_x(Na_{0.5}K_{0.5})_{1-x}]\ NbO_3$ exhibits orthorhombic structure for $x \leq 0.05$ and transformed to tetragonal structure for $x \geq 0.07$. The Li substitution at A-sites (Na, K) in NKN ceramics lowers T_{O-T} from 200^0C to near room temperature and raises T_C from 420^0C to about 500^0C.[38] However, the opposite effect in case of HB-LNKN [Fig. 3(a)] suggests the reduction of Li content as

compared to that in the AS-LNKN. The increase in Li content in the system (1-*x*) $(Na_{0.535}K_{0.48})NbO_3$-*x*$LiNbO_3$ (*x* = 0.058 - 0.090) has been shown to change the structure from orthorhombic to tetragonal phase with the two phase coexistence region at *x* = 0.070 - 0.080.[39] Wongsaenmai et al.[40] demonstrated that in $[(K_{0.5}Na_{0.5})_{1-x}Li_x]NbO_3$ ceramic system, the morphotropic phase boundary between two phases were obtained at x = 0.06 - 0.065. The study also suggests that with increase in Li content, T_C shifts towards higher temperature region.[40] In addition to the Li content, the processing parameter also plays an important role in phase transformation in LNKN ceramics due to the volatilization of alkali components during high temperature sintering.[41] However, in the present study, the samples were processed at similar conditions. It can therefore be suggested that the variation in dielectric and electrical properties of HB-LNKN samples is attributed to the variation in Li content. The electrical properties can be altered significantly by compositional modifications in LNKN ceramics.[42]

In summary, the physical and electrical characteristics of the laminated composite samples for the buffer layer composition of X = 7 is observed to be optimal. Therefore, the laminated composite with the buffer composition, X = 7 has been taken as optimized sample for evaluating the electrical properties as well as surface charge induced *in-vitro* bioactivity.

3.3 Electrical Properties of the laminated HA-buffer-LNKN-buffer-HA composite

Fig. 9 shows the variation of polarization and current density with electric field for the laminated composite with buffer layer composition, X = 7. The PE hysteresis loop reveals poor saturation characteristic because of the increased space charge region due to the layered configuration. However, for the HB-LNKN sample, the hysteresis curve demonstrated clear saturation (Fig. 5). The peak due to domain reversal is observed in the current density versus electric field plot at an applied field of about 30 kV/cm (Fig.9).[43] The domain reversal suggests that the LNKN

interlayer can be polarized, despite of being laminated with buffer and HA layers in the composite.

The dielectric constant and loss for the laminated composite sample are measured to be 60 and 0.06, respectively. After corona polarization, the dielectric constant increased to 93 with the significant reduction in dielectric loss value (0.02). Also, the piezoelectric strain coefficient (d_{33}) for the polarized laminated composite is obtained to be 2.0 pC/N. The piezoelectric coefficient (d_{14}) for the living bone has been reported to be 0.7 pC/N.[44] The dielectric constant of monolithic HA phase is about 10, which has been increased by 6 folds in the developed laminated composite. The corona poling further increases the dielectric constant of laminated composite by about 1.5 fold.

The schematic (Fig. 10) illustrates one of the possible mechanisms for improved polarization of HA by the proposed concept of laminated composite. The spontaneous electrical polarization of LNKN (from the middle as well as buffer layers) may induce polarization in HA layer. As the applied mechanical stress can be converted into electrical energy by virtue of piezoelectricity of LNKN, such laminated composite is expected to provide the mechanical strength to HA as well. Overall, the electrical and mechanical response of HA can be improved significantly without affecting its biocompatibility through the developed laminated composite. Further, the effect of increased polarizability of hydroxypatite on the *in vitro* bioactivity has been examined.

3.4 *In vitro* bioactivity evaluation

The *in vitro* bioactivity for the unpolarized and corona polarized laminated composite samples (for X = 7) was evaluated after immersing in SBF for 3, 7 and 14 days, respectively. For comparing the result, as-sintered HA samples were also examined in similar conditions. The XRD results confirmed the formation of single phase HA in both the samples (not shown).

Electron probe micro-analyses (EMPA) confirmed the Ca/P ratios in HA and laminated composite surfaces are almost same (~ 1.7).

Fig. 11 plots the XRD patterns of the laminated composite samples, before and after immersion in SBF for 3, 7 and 14 days, respectively. The XRD analyses reveal the presence of the amorphous calcium phosphate (ACP) on the surface of the soaked sample after 3 days of immersion in SBF. The intensity of the peak corresponding to ACP phase decreased with further increase in the soaking duration. After 14 days of immersion, the broadness in the diffraction peaks suggest the formation of apatite with low crystallinity. The ACP has been converted to low crystalline apatite through Ca uptake from SBF with increase in the soaking duration of up to 14 days.[45]

Fig. 12 demonstrates the variation in the thickness of the apatite layer, formed on as-sintered HA as well as unpolarized, positively and negatively polarized laminated composite samples, with soaking duration (in SBF). From the figure, it is clear that the thickness of the apatite layer on the laminated composite increased significantly on the laminated composites as compared to that on as-sintered HA. The rate of formation of apatite layer on unpolarized and polarized laminated composite HA-LNKN-HA surfaces are about 0.8 μm/day, which is double to that on the HA surface (0.4 μm/day). Although, the precise measurement of apatite layer thickness is difficult, this result suggests that the laminated composites can improve *in vitro* bioactivity significantly. The improvement in electrical polarizability of HA after incorporating LNKN layer between HA layers can be suggested as one of the possible reasons for the increased apatite formation rate on the laminated composites.

The increase in bioactivity by the polarized surfaces depends on the nature of polarity. The negatively charged surfaces increase the *in vitro* bioactivity via preferred adsorption of Ca^{2+} ions

from SBF, which serve as nuclei to form apatite layer with the anions HPO_4^{2-} and OH^-.[46] However, the positively charged surfaces do not provide such favorable environment. Yamashita et al.[23] also demonstrated that the negatively charged surface of HA accelerates and positively polarized side decelerates the bone-like crystal growth. Negatively charged surfaces increase wettability as well as facilitates better electrostatic interaction of Ca^{2+} ions, which led to the accelerated growth of apatite crystals.[24] It has been reported that irrespective of charge polarity, the polarized surfaces increase the wettability.[47] Gu et al.[48] suggested that HA surface favors the development of apatite layer by ion exchange mechanism with the simulated body fluid, which enhances the activity product of the Ca^{2+} and PO_4^{3-} ions. The formation of calcium-phosphate (Ca-P) layer on the negatively charged surfaces depends on the poling conditions. The Ca/P ratio on the negatively charged surfaces of the piezoelectric $BaTiO_3$, poled (at 85^0C) below its Curie temperature (120^0C), is reported in the range of 1.2-1.5. However, poling (at 160^0C) above Curie temperature led to Ca/P ratio in the range of 1.5-1.67.[49] Also, polarized piezoelectric ceramic demonstrate anisotropy in crack propagation in different loading conditions.[50] The ceramic exhibits higher resistance for the crack to propagate along the polarization direction as compared to normal to the polarization direction. In an *in vivo* study by Jianqing et al.[51], it has been demonstrated that the electrical potential generated due to the applied mechanical stress on the piezoelectric bioceramic promotes osteogenesis. In addition to the polarized surfaces, the application of external electrical potential also enhances the biomineralization through the biochemical stimulation of the osteoblast-like cells.[52] However, in the present study, a comparison between unpolarized and polarized laminated composite samples suggests that there is no significant difference in the apatite formation rate between the charged and uncharged

surfaces which is probably associated with the insufficient charge induction due to the corona polarization.

Nevertheless, the present study do establish the significant increase in dielectric and electrical properties as well as *in vitro* bioactivity of HA by incorporating the ferroelectric LNKN interlayer between HA layers.

4. Conclusions

The present study demonstrated the consequences of incorporation of ferroelectric LNKN layers between the HA sheets through the buffer interlayer in terms of the considerable improvement in electrical activities as well as *in vitro* bioactivity of HA. The insertion of buffer layers avoid the sharp interface between HA and LNKN layers as well as provides the better adhesion between the layers. The crystal structure of the incorporated LNKN layer has been changed from tetragonal to orthorhombic phase. In addition, the tetragonal region, i.e., the range between T_{O-T} and T_C has also been reduced for the incorporated LNKN layer as compared to as-sintered LNKN, which is found to dependent upon the composition of the buffer layer in the laminated composite.

The polarizability of HA has been increased by more than 6 fold with the proposed concept of laminated composite. The spontaneous polarization of the LNKN interlayer is probably responsible for the increased polarizability of HA. Also, the developed laminated composite is piezoelectric in nature, like that of the living bone. Overall, the significant electrical activities and higher rate of apatite formation suggest that the developed laminated composite can be a prospective substitute for electro-active orthopedic implants.

Acknowledgements

We gratefully acknowledge the financial support by Grant-in-Aids for JSPS Challenging Exploratory Research (No.2365400) and for the JSPS Fellows (No.24-2377).

References

[1] M.P. Ferraz, F.J. Monteiro and C.M. Manuel. *J. Appl. Biomater. Biom.*, 2004, **2**, 74.

[2] Q. Liu, S. Huang, J.P. Matinlinna, Z. Chen and H. Pan. *Biomed. Res. Int.*, 2013, **2013**, 1.

[3] R. Astala and M.J. Stott. *Chem. Mater.*, 2005, **17**, 4125.

[4] S.V. Dorozhkin. *Materials*, 2009, **2**, 399.

[5] L.L. Hench. *J. Am. Ceram. Soc.*, 1991, **74**(7), 1487.

[6] R. Garcia and R.H. Doremus. *J. Mater. Sci.-Mater. Med.*, 1992, **3(**2), 154.

[7] I. Yasuda. *J. Japanese Orthop. Surg. Soc.*, 1954, **28** (3), 267.

[8] E. Fukada and I. Yasuda. *J. Phys. Soc. Jap.*, 1957, **12**, 1158.

[9] S.B. Lang. *Nature*, 1966, **212**,704.

[10] M.A. EI Messiery, G.W. Hastings and S. Rakawski. *J. Biomed. Eng.*, 1979, **1**, 63.

[11] C.J. Dreyer. *Nature*, 1961, **189**, 594.

[12] G.W. Hastings and F.A. Mahmud. *J. Biomed. Eng.*, 1988, **10**, 515.

[13] Z.B. Friendenberg, R. Dyer, and C.T. Brighton. *J. Dent. Res.*, 1971, **50**, 635.

[14] F.R. Baxter, C.R. Bowen, I.G. Turner and A.C.E. Dent. *Ann. Biomed. Eng.*, 2010, **38**(6), 2079.

[15] G.W. Hastings, M.A. ElMessiery and S. Rakowski. *Biomater.*, 1981, **2**, 225.

[16] A.A. Marino and R.O. Becker. *Nature*, 1970, **228**, 473.

[17] C.A. Bassett and R.O. Becker. *Science*, 1962, **137**(3535), 1063.

[18] J.H. McElhaney. *J. Bone Joint Surg. Am.*, 1967, **49**, 1561.

[19] T. Kobayashi, S. Nakamura and K.Yamashita. *J. Biomed. Mater. Res.*, 2001, **57**, 477.

[20] S. Nakamura, T. Kobayashi and K.Yamashita. *J. Biomed. Mater. Res. A*, 2004, **68**, 90.

[21] A. Huttenlocher and A.R. Horwitz. *N. Engl. J. Med.*, 2007, **356**(3), 303.

[22] A.P.R. Lirani-Galvao, C.T. Bergamaschi, O.L. Silva, and M. Lazaretti-Castro. *Braz. J. Med. Biol. Res.*, 2006, **39**, 1501.

[23] K. Yamashita, N. Oikawa and T. Umegaki. *Chem. Mater.*, 1996, **8**, 2697.

[24] S. Bodhak, S. Bose and A. Bandyopadhyay. *Acta Biomat.*, 2009, **5**, 2178.

[25] J.B. Park, B.J. Kelly, G.H. Kenner, A.F. von Recum, M.F. Grether, W.W. Coffeen. *J. Biomed. Mater. Res.*, 1981, **15**(1), 103.

[26] J.B. Park, A.F. von Recum, G.H. Kenner, B.J. Kelly, W.W. Coffeen and M.F. Grether. *J. Biomed. Mater. Res.*, 1980, **14**(3), 269.

[27] X.M. Chen and B.Yang. *Mater. Lett.*, 1997, **33**, 237.

[28] B. Yang and X.M. Chen. *J. Eur. Ceram. Soc.*, 2000, **20**, 1687.

[29] K. Kakimoto, Y. Hayakawa and I. Kagomiya. *J. Am. Ceram. Soc.*, 2010, **93**(9), 2423.

[30] K. Nilsson, J. Lidman, K. Ljungstrom and C. Kjellman, "Biocompatible material for implans, U.S. patent 6,526,984 B1 (2003).

[31] R. Olivares-Navarrete, J.J. Olaya, C. Ramirez and SE.Rodil. *Coatings*, 2011, **1**, 72.

[32] Y. Guo, K. Kakimoto and H. Ohsato. *Appl. Phys. Lett.*, 2004, **85**(18), 4121.

[33] A.K. Dubey, H. Yamada and K. Kakimoto. *J. Appl. Phys.*, 2013, **114**, 124701.

[34] H.M. Kim, F. Miyaji, T. Kokubo, S. Nishiguchi and T. Nakamura, *J. Biomed. Mater. Res.*, 1999, **45**, 100.

[35] T. Kokubo, H. Kushitani, S. Sakka, T. Kitsugi and T. Yamamum, *J. Biomed. Mater. Res.*, 1990, **24**, 721.

[36] S. Reddy, A.K. Dubey, B. Basu, R. Guo, and A.S. Bhalla. *Int. Ferroelectr.*, 2011, **131**(1), 147.

[37] K. Shibata, K. Suenaga, A. Nomoto and T. Mishima. *Jpn. J. Appl. Phys.*, 2009, **48**, 121408.

[38] K. Kakimoto, T. Sumi and I. Kagomiya, *Jpn. J. Appl. Phys.*, 2010, **49**, 09MD10.

[39] K. Wang, J.F. Li and N. Liu, *Appl. Phys. Lett.*, 2008, **93**, 092904.

[40] S. Wongsaenmai, S. Ananta and R. Yimnirun, Effect of Li addition on phase formation behavior and electrical properties of $(K_{0.5}Na_{0.5})NbO_3$ lead free ceramics, *Ceram. Int.*, 2012, **38**, 147.

[41] P. Zhao, B. P. Zhang and J. F. Li, *Appl. Phys. Lett.*, 2007, **90**, 242909.

[42] P. Zhao, B.P. Zhang and J.F. Li, *Appl. Phys. Lett.*, 2007, 91, 172901.

[43] H. Banno. *Ceram. Bull.*, 1987, **66**, 1332.

[44] J.B. Park and R.S. Lakes, "Biomaterials: an Introduction," Plenum, New York ,1992.

[45] E. Beniash, R.A. Metzler, R.S. Lam and P.U. Gilbert. *J. Struct. Biol.*, 2009, **166**, 133.

[46] Y. J. Park, K. S. Hwanga, J. E. Song, J. L. Ong and H. R. Rawls. *Biomaterials*, 2002, **23**,3859.

[47] A. K. Dubey and B. Basu. *J. Am.Cer. Soc.*, 2014, **97**(2), 481.

[48] Y.W. Gu, K.A. Khor, P. Cheang. *Biomaterials*, 2004, **25**, 4127.

[49] K. S. Hwang, J. E. Song, H.S. Yang, Y. J. Park, J. L. Ong and H. R. Rawls. *J. Mater. Sc. Mater. Med.*, 2002, **13**, 133.

[50] H. Wang and R. N Singh, *Ferroelectr.*, 1998, **207**, 555.

[51] F. Jianqing, Y. Huipin and Z. Xingdong, *Biomaterials*, 1997, **18**, 1531.

[52] H. P. Wiesmann, M. Hartig, U. Stratmann, U. Meyer and U. Joos, *Biochim. Biophys. Acta*, 2001, **1538**, 28.

Legends

List of Tables:

Table 1: The dielectric and electrical properties of LNKN, obtained after removing HA and buffer layers from the parent laminated composites (HB-LNKN).

List of Figures:

Fig. 1 (a): SEM image of cross section of the HA-buffer-LNKN-buffer-HA laminated composite demonstrating Ca diffusion at the buffer (X = 7) and LNKN interface.

Fig. 1 (b): Variation in the thickness of reaction layer with the various buffer layer compositions.

Fig. 2(a): The XRD patterns of as-sintered LNKN (AS-LNKN) and the LNKN, obtained after removing the HA and buffer layers from the laminated composite (HB-LNKN). The patterns for HB-LNKN is shown for various buffer layer compositions (X = 1~9) in the parent laminated composite.

Fig. 2 (b): XRD patterns of stoichiometric and A-site deficient NKN as well as the LNKN, obtained after removing HA and buffer layers from the laminated composite (HB-LNKN).

Fig. 3 (a): Variation of dielectric constant with temperature for as-sintered LNKN (AS-LNKN) as well as LNKN, obtained after removing the HA and buffer layers from the laminated composite (HB-LNKN).

Fig. 3 (b): Variation of tetragonal region (difference between T_C and T_{O-T}) of LNKN, obtained after removing the HA and buffer layers from the laminated composite (HB-LNKN), with the molar ratio (X) of LNKN in the buffer layer of the parent laminated composite.

Fig. 4: Variation of electrical resistivity of LNKN, obtained after removing the HA and buffer layers from the laminated composite (HB-LNKN), as a function of molar ratio (X) of LNKN in the buffer layer of the parent laminated composite.

Fig. 5: The PE hysteresis loops for as-sintered LNKN (AS-LNKN) as well as LNKN, obtained after removing the HA and buffer layers from the laminated composite (HB-LNKN). (b)-(f) demonstrate the hysteresis loops for HB-LNKN with various molar ratios (X = 1~9) of LNKN in the buffer layer of the parent laminated composite.

Fig. 6 (a): Variation of dielectric constant and loss with frequency for LNKN, obtained after removing the HA and buffer layers from the laminated composite (HB-LNKN). The plots for the various molar ratios (X) of LNKN in the buffer layer of the parent laminated composite are shown.

Fig. 6 (b): The dielectric constant and loss for HB-LNKN as a function of the molar ratios (X) of LNKN in the buffer layer of the parent laminated composite, measured at 1 kHz of frequency.

Fig. 7: The piezoelectric strain coefficient (d_{33}) of LNKN, obtained after removing the HA and buffer layers from the laminated composite (HB-LNKN), as a function of the molar ratios (X) of LNKN in the buffer layer of the parent laminated composite.

Fig. 8: The XRD patterns of LNKN, obtained after removing the HA and buffer layers from the laminated composite (HB-LNKN), with the thicknesses of 1 and 0.5 mm.

Fig. 9: Variation of polarization and current density with electric field for the laminated composite with the buffer layer composition, X = 7.

Fig. 10: Schematic illustrating one of the possible mechanisms for increased polarizability of HA in the laminated composite.

Fig. 11: The XRD patterns of the biomineralized surfaces of HA-LNKN-HA laminated composite after immersion in SBF for 3, 7 and 14 days, respectively.

Fig. 12: Variation in the thickness of the apatite layer on HA, unpolarized and polarized laminated HA-LNKN-HA composite as a function of immersion time in SBF.

Tables

Table 1: The dielectric and electrical properties of LNKN, obtained after removing HA and buffer layers from the parent laminated composites (HB-LNKN).

Buffer Composition	Thickness (mm)	ε_r (@ 1 kHz)	tan δ (@ 1 kHz)	ρ (Ω cm)	d_{33} (pC/N)
X = 6	1	555	0.09	2.0×10^9	86
	0.5	513	0.06	1.5×10^{10}	136
X = 7	1	581	0.10	2.0×10^9	104
	0.5	584	0.08	2.1×10^{10}	145

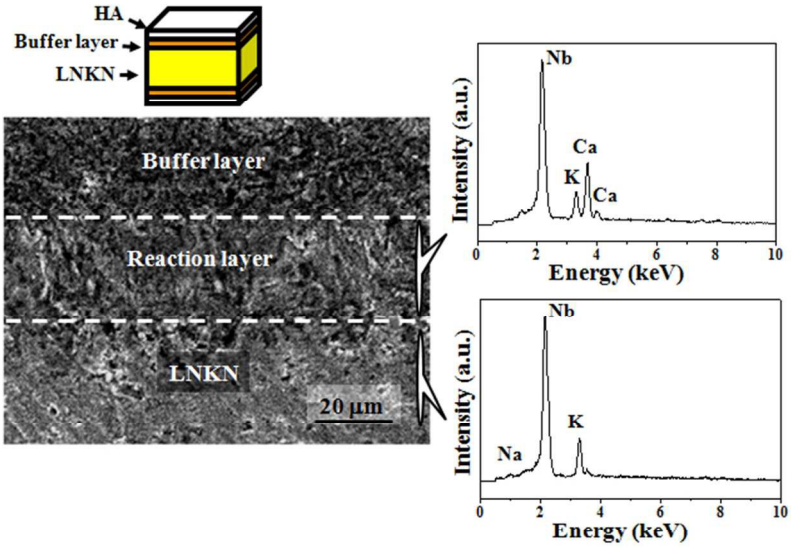

Fig. 1 (a): SEM image of cross section of the HA-buffer-LNKN-buffer-HA laminated composite demonstrating Ca diffusion at the buffer (X = 7) and LNKN interface.
67x50mm (300 x 300 DPI)

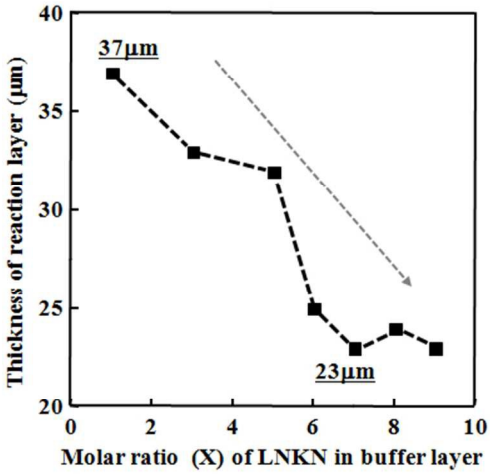

Fig. 1 (b): Variation in the thickness of reaction layer with the various buffer layer compositions.
67x50mm (300 x 300 DPI)

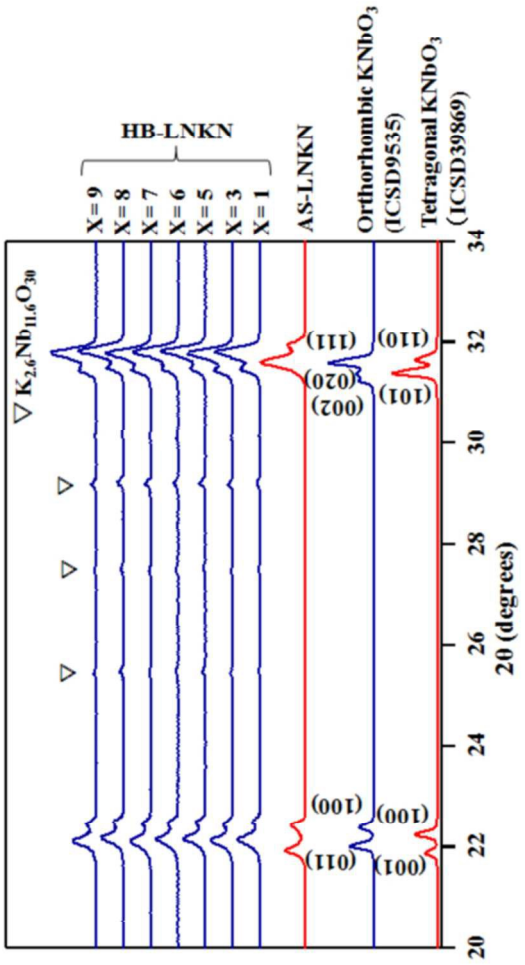

Fig. 2(a): The XRD patterns of as-sintered LNKN (AS-LNKN) and the LNKN, obtained after removing the HA and buffer layers from the laminated composite (HB-LNKN). The patterns for HB-LNKN is shown for various buffer layer compositions (X = 1~9) in the parent laminated composite.
84x91mm (300 x 300 DPI)

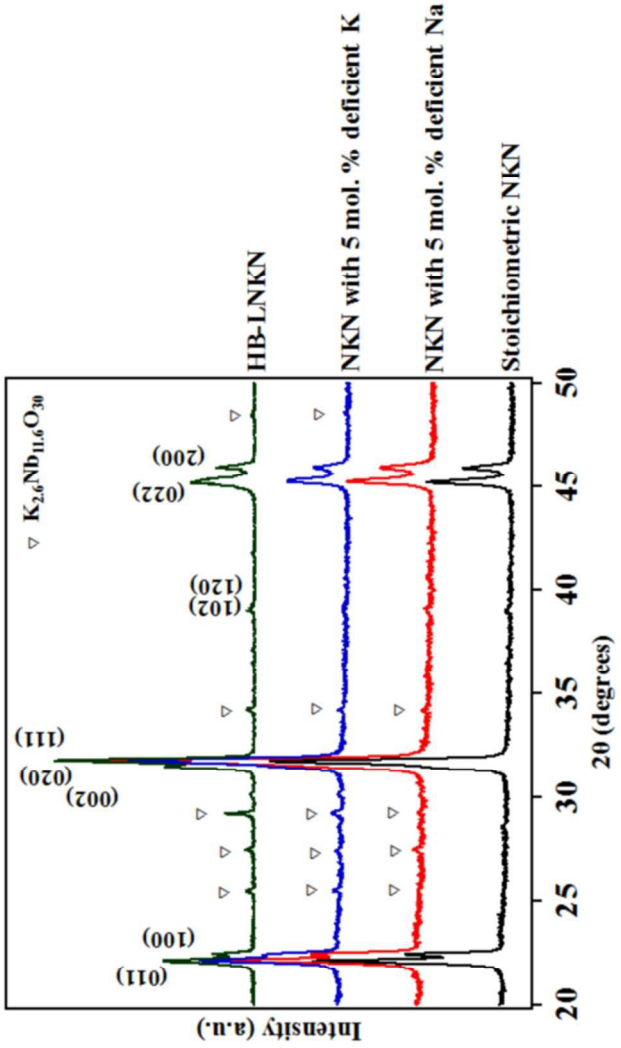

Fig. 2 (b): XRD patterns of stoichiometric and A-site deficient NKN as well as the LNKN, obtained after removing HA and buffer layers from the laminated composite (HB-LNKN).
84x91mm (300 x 300 DPI)

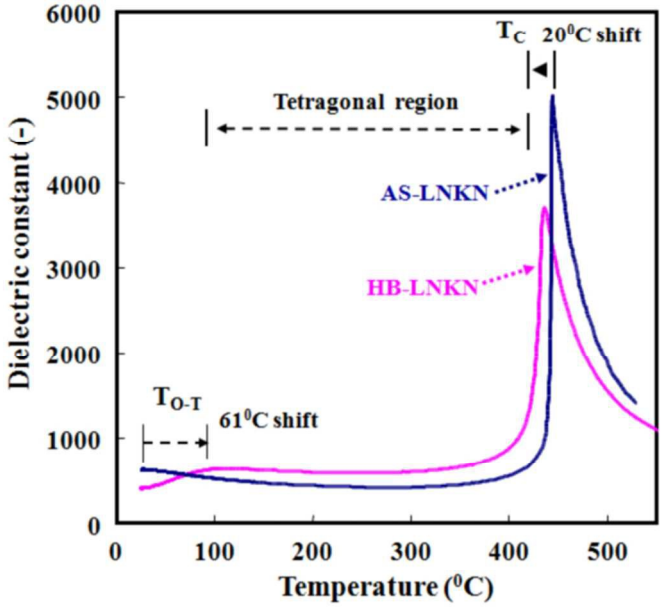

Fig. 3 (a): Variation of dielectric constant with temperature for as-sintered LNKN (AS-LNKN) as well as LNKN, obtained after removing the HA and buffer layers from the laminated composite (HB-LNKN).
84x63mm (300 x 300 DPI)

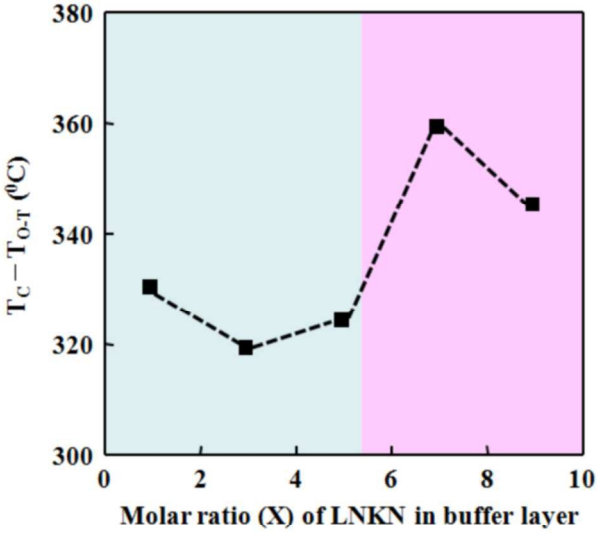

Fig. 3 (b): Variation of tetragonal region (difference between TC and TO-T) of LNKN, obtained after removing the HA and buffer layers from the laminated composite (HB-LNKN), with the molar ratio (X) of LNKN in the buffer layer of the parent laminated composite.
143x107mm (300 x 300 DPI)

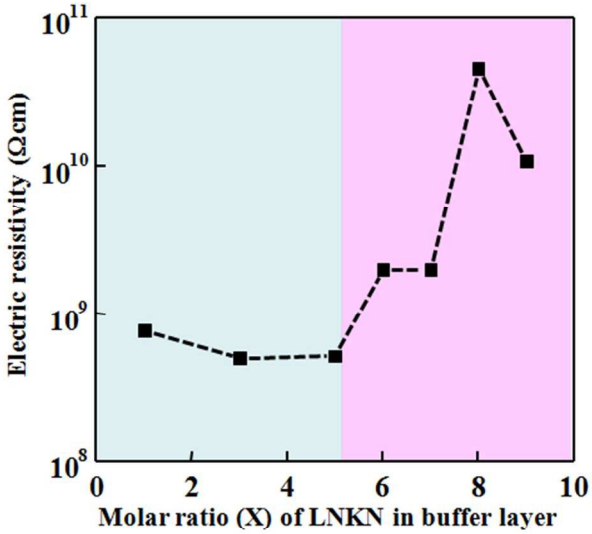

Fig. 4: Variation of electrical resistivity of LNKN, obtained after removing the HA and buffer layers from the laminated composite (HB-LNKN), as a function of molar ratio (X) of LNKN in the buffer layer of the parent laminated composite.
67x50mm (300 x 300 DPI)

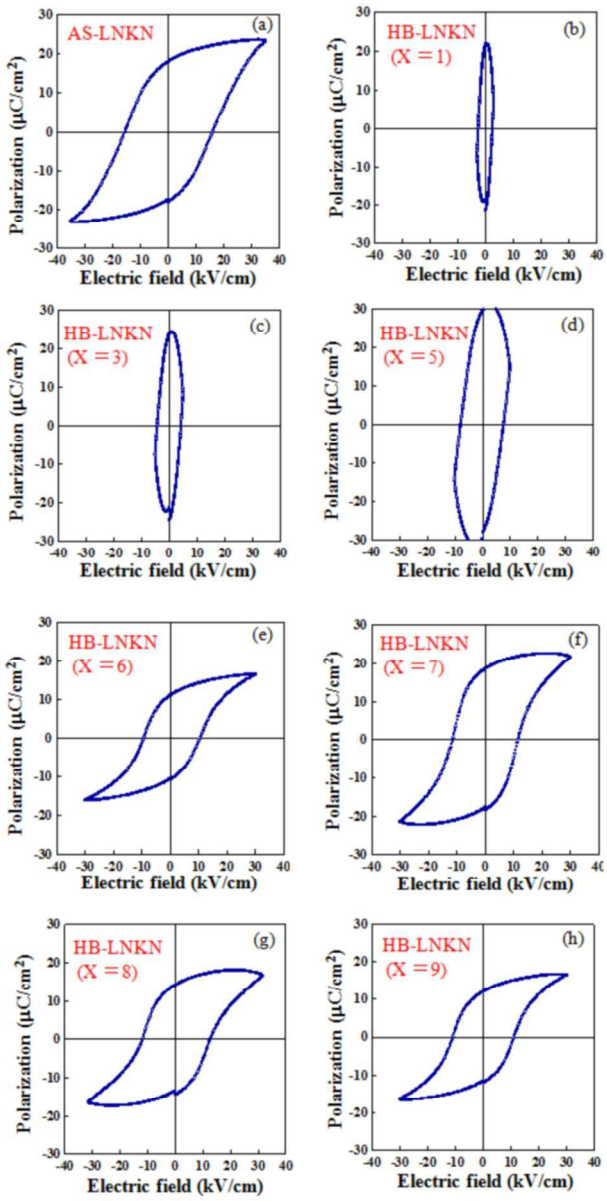

Fig. 5: The PE hysteresis loops for as-sintered LNKN (AS-LNKN) as well as LNKN, obtained after removing the HA and buffer layers from the laminated composite (HB-LNKN). (b)-(f) demonstrate the hysteresis loops for HB-LNKN with various molar ratios (X = 1~9) of LNKN in the buffer layer of the parent laminated composite.
169x210mm (300 x 300 DPI)

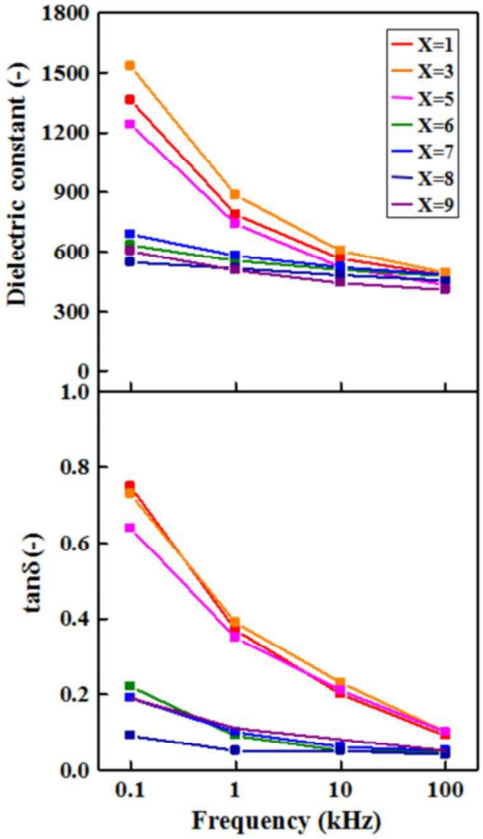

Fig. 6 (a): Variation of dielectric constant and loss with frequency for LNKN, obtained after removing the HA and buffer layers from the laminated composite (HB-LNKN). The plots for the various molar ratios (X) of LNKN in the buffer layer of the parent laminated composite are shown.
84x73mm (300 x 300 DPI)

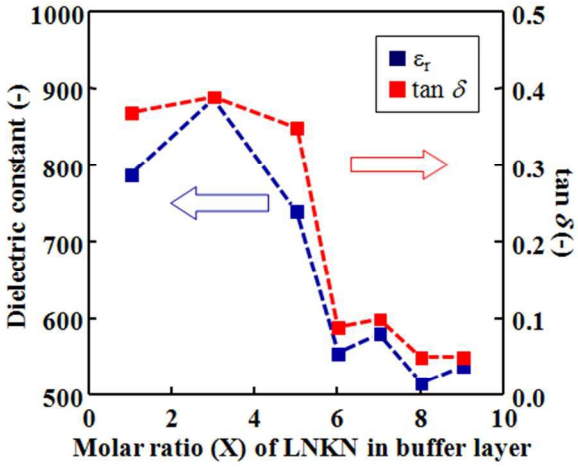

Fig. 6 (b): The dielectric constant and loss for HB-LNKN as a function of the molar ratios (X) of LNKN in the buffer layer of the parent laminated composite, measured at 1 kHz of frequency.
67x50mm (300 x 300 DPI)

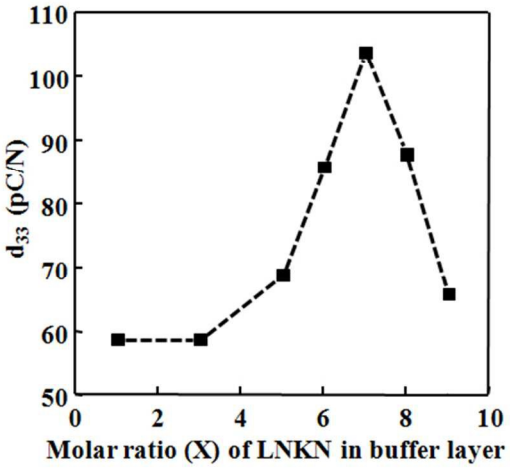

Fig. 7: The piezoelectric strain coefficient (d33) of LNKN, obtained after removing the HA and buffer layers from the laminated composite (HB-LNKN), as a function of the molar ratios (X) of LNKN in the buffer layer of the parent laminated composite.
67x50mm (300 x 300 DPI)

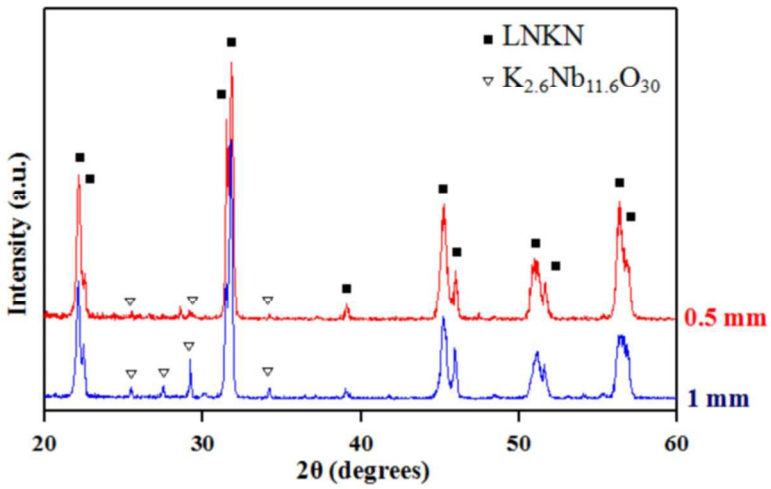

Fig. 8: The XRD patterns of LNKN, obtained after removing the HA and buffer layers from the laminated composite (HB-LNKN), with the thicknesses of 1 and 0.5 mm.
84x63mm (300 x 300 DPI)

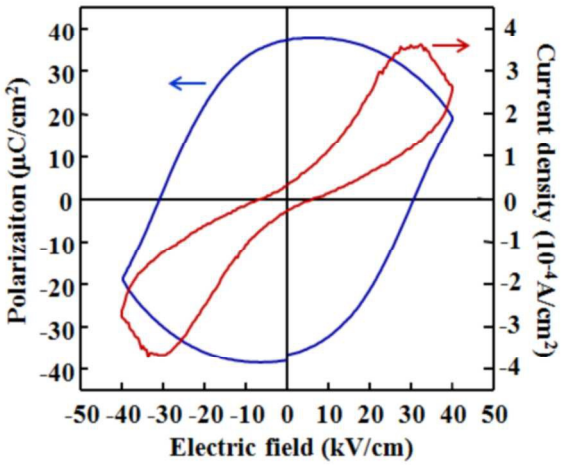

Fig. 9: Variation of polarization and current density with electric field for the laminated composite with the buffer layer composition, X = 7.
194x146mm (300 x 300 DPI)

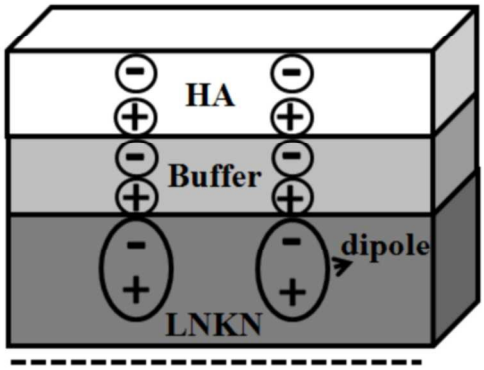

Fig. 10: Schematic illustrating one of the possible mechanisms for increased polarizability of HA in the laminated composite.
194x146mm (300 x 300 DPI)

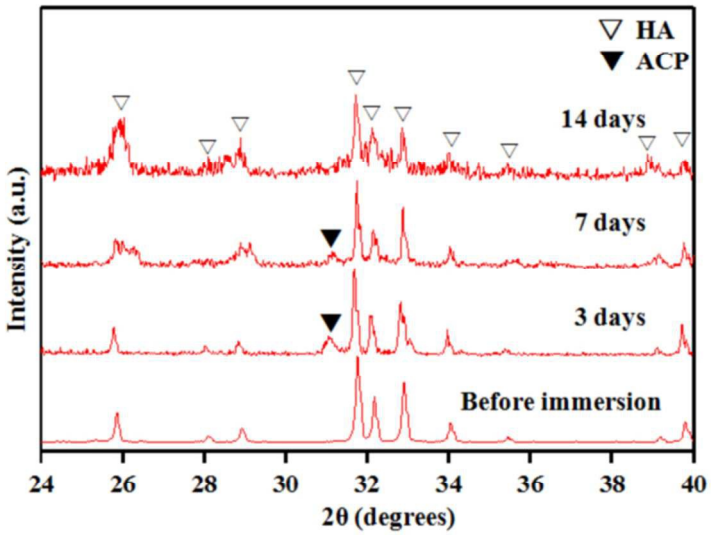

Fig. 11: The XRD patterns of the biomineralized surfaces of HA-LNKN-HA laminated composite after immersion in SBF for 3, 7 and 14 days, respectively.
84x63mm (300 x 300 DPI)

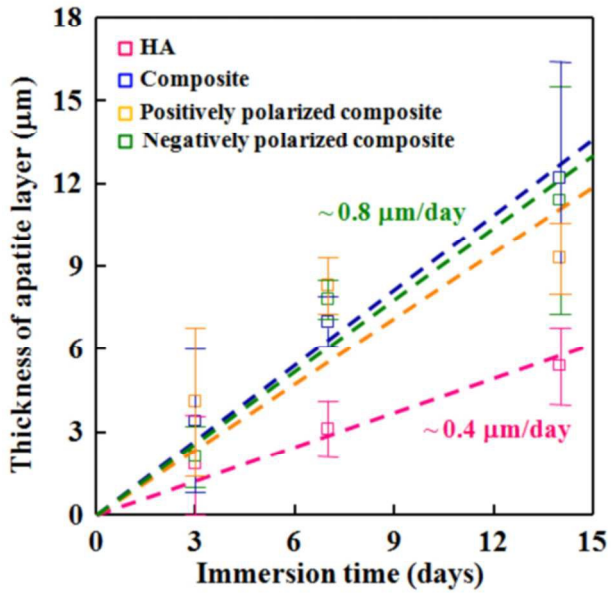

Fig. 12: Variation in the thickness of the apatite layer on HA, unpolarized and polarized laminated HA-LNKN-HA composite as a function of immersion time in SBF.
84x63mm (300 x 300 DPI)